18TH WORLD CONFERENCE ON EARTHQUAKE ENGINEERING
WCEE2024
MILAN

MILAN, ITALY
30TH JUNE - 5TH JULY 2024
www.wcee2024.it

INTEGRATION OF MULTI-SOURCE AND POST-EVENT DATA INTO EMS-98 BASED EARTHQUAKE DAMAGE ANALYSIS

N. Hadidian M.[1], J. Schwarz[2]

[1] Research Assistant in Earthquake Damage Analysis Center (EDAC),
Bauhaus Universität Weimar, Germany, nooshin.hadidian.moghaddam@uni-weimar.de

[2] Head of Earthquake Damage Analysis Center (EDAC), Bauhaus Universität Weimar,
schwarz@uni-weimar.de

Abstract: *A systematic and high-quality framework for building data inventory collection streamlines the procedures for fast, unified post-hazard risk assessment with an appropriate level of certainty. This paper explores a systematic framework for post-earthquake analysis, taking the L'Aquila, Italy earthquake on 6 April 2009 with Mw=6.3 as a case study. The method integrates multi-source building data collection methodologies, encompassing ground surveys, Google Street-view, and Very High Resolution (VHR) satellite imagery. Vulnerability and damage grade assessments from ground surveys conducted by Italian researchers are cross-referenced with Google 3D views (where available and accessible) and changes detected through VHR satellite image processing. Several approaches are employed, based on selected algorithms for both automatic/semi-automatic and visual inspection methods, utilizing various tools.*

For the visual inspection methods, seven criteria have been established and evaluated to shape the model of damage grade assessment using VHR satellite images. This model aligns closely with the EMS-98 definitions, which serve as a validated code for ground truth approaches, addressing both structural and non-structural elements of buildings for each designated damage level. Several algorithms in automatic change detection procedures are deployed to pinpoint areas with concentrated high damage grades (primarily D5), as verified by ground surveys and visual inspection methods on VHR satellite images.

The results derived from this multi-source data collection approach, offer an appropriate sureness level for the established seven criteria used in damage grade assessment via VHR satellite images. This method can serve as an integrated evaluation system, facilitating the examination of damage assessment accuracy against ground truth benchmarks in various case studies. Moreover, the integration of these criteria into the visual inspection method can mitigate the challenges of vertical view limitations in detecting lower damage grades, as per the EMS-98 scales. It can also establish a unified, engineered framework for earthquake damage analysis, even when a clear horizontal view of the investigated zone is absent.

1. Introduction

Validating a systematic framework for building data evaluation, particularly when using vertical satellite or aerial images, poses a significant challenge in geo-spatial rapid response assessment. The application of automatic methodologies to remote sensing images for change detection analysis in the aftermath of natural hazards, such as earthquakes, primarily focuses on district-level damage recognition in urban contexts. In

many cases, the assigned damage levels do not align with the defined scales in EMS-98 for earthquake assessment.

This study places emphasis on introducing an engineered criteria-based framework for post-earthquake building damage assessment using vertical very high-resolution (VHR) satellite images in the city of L'Aquila following the 6.3 Mw earthquake in April 2009.

Numerous studies have been conducted in the field of damage grade assessment, utilizing both ground surveys and remote sensing images. Tertulliani *et al.* (2011) described the distribution of vulnerability and damage levels in buildings following this earthquake, using the EMS-98 definitions, which were verified through ground truth evaluations. Contreras *et al.* (2015) employed an integrated approach, combining remote sensing, GIS, and ground observations, to study the identification of damaged areas in city districts and monitor the recovery progress following an earthquake in the city of L'Aquila. Meanwhile, Kersten *et al.* (2017) scrutinized the application of remote sensing stand-alone tools by using object-based analysis on satellite images to detect changes in buildings after an earthquake. De Vecchi and Dell'Acqua (2014) conducted a study in L'Aquila city to explore the benefits of integrating crowd-sourced information with spaceborne images for identifying seismic damages on buildings. Their research demonstrates improvements in accuracy for risk assessment. Another study by Maiwald and Schwarz (2020) is conducted to evaluate the observed damages in L'Aquila using simulative earthquake damage modeling based on EMS-98 reliability and predictability.

The responsible author of this paper developed the EMS-98 criteria-based framework -also see Hadidian and Schwarz (2022), which was applied to Very High-Resolution (VHR) satellite images to compare the distribution of damage grades in the city of L'Aquila with the findings of previous scientific studies. Additionally, this method was complemented with the use of Google Street View (if accessible) to assess building stock survey parameters, including structural type, number of stories, and vulnerability classes. The method exhibited significantly higher accuracy compared to ground surveys. Furthermore, the subsequent sections will provide explanations for the uncertainties and questions surrounding certain aspects of the ground survey results.

In the following steps, the results of automatic/semi-automatic approaches employing various algorithms are compared with the outcomes of the criteria-based framework used in the visual inspection method on Very High-Resolution (VHR) satellite images and evaluated damage distribution through ground surveys in the city of L'Aquila.

2. Acquisition of space borne and ground survey data

Visual inspection was conducted on two temporal VHR QuickBird satellite images with the following specifications:

1. The pre-earthquake image, captured on 4 September 2006, featured a spatial resolution of 60 cm, zero cloud cover, and was in the 4-band pansharpened format.
2. The post-earthquake image, taken on 8 April 2009, had a spatial resolution of 60 cm, zero cloud cover, and was in the 4-band pansharpened format.

Figure 1 illustrates the visual comparison of the pre- and post-event images.

The assigned vulnerability class and damage grades, as determined by Tertulliani *et al.* (2011), served as the results of the ground survey assessment.

In the application of automatic/semi-automatic methods and for result comparison, various tools including QGIS, ERDAS-IMAGINE, and MATLAB were utilized. These tools were selected based on their compatibility with different mathematical algorithms.

In following steps, the evaluated vulnerability class and damage grade of buildings are compared between ground survey and EMS-98 criteria-based framework on VHR satellite images and the difference of measurements are quantified with several methods. The accuracy level of ground survey results is scrutinized using several visual examples and analysis.

Further, the analysed outcomes from automatic/semi-automatic image processing methods are compared with evaluated damage grades of buildings by both ground survey and visual investigation on VHR satellite images.

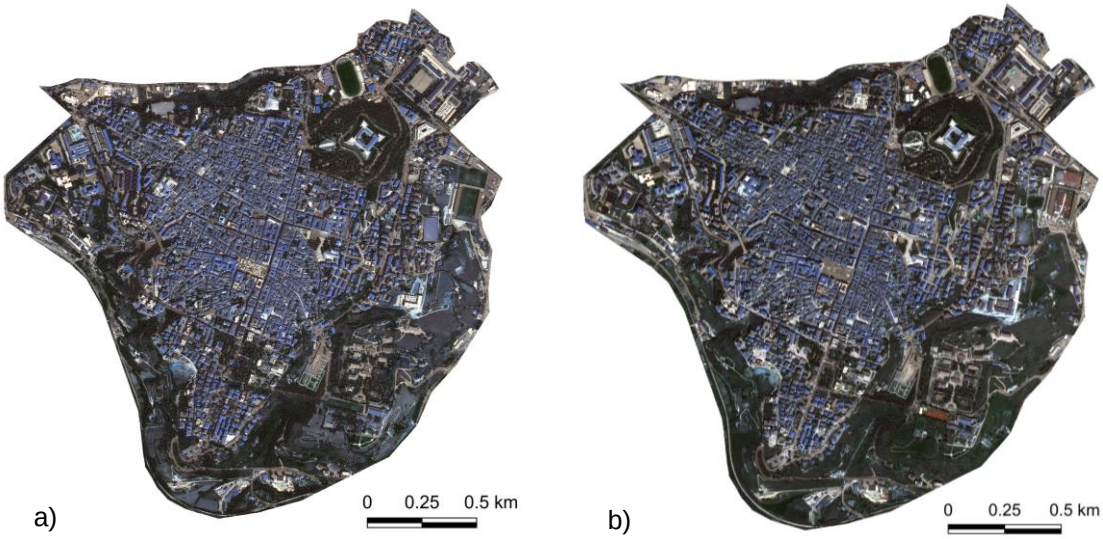

Figure 1. VHR images of L'Aquila a) Pre-event and b) Post-event

3. Methodologies

3.1. Visual inspection on VHR satellite images

Many studies have attempted to apply EMS-98 by Grünthal *et al.* (1998) for post-earthquake damage assessment on satellite images through visual interpretation. Examples include the work of Corbane *et al.* (2011) and UNOSAT (2010) for the 2010 M7 earthquake in Haiti, as well as the study by Yamazaki *et al.* (2005) on the 2003 6.6 Mw earthquake in the city of Bam, Iran.

In the case of Haiti, damage grades were primarily assessed based on detected debris and visible evidence of complete or partial building collapses. However, the certainty levels associated with the assigned damage grades were not evaluated. For Bam, damage assessment was categorized into grades D5, D4, D3, and D2-1. The confusion matrix for several selected districts revealed both omission and commission errors.

Consequently, there is an essential need to develop a systematic and engineered framework for the visual interpretation method on Very High-Resolution (VHR) satellite images. This framework would aim to establish better compatibility with EMS-98 criteria used in ground survey inspections. The schematic format of EMS-98 criteria-based framework is shown in Figure 2.

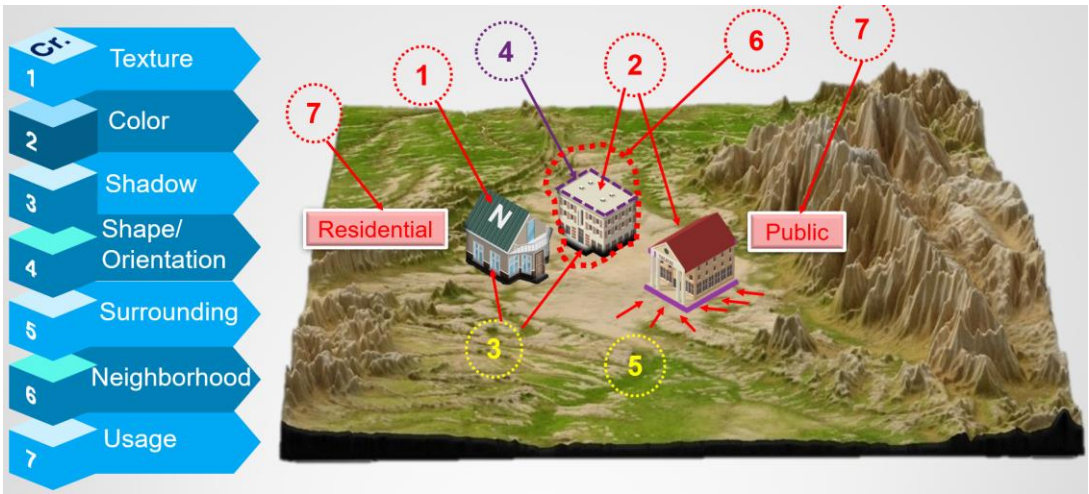

Figure 2. Schematic format of defined criteria for damage grade evaluation in visual interpretation on VHR satellite images

*-*N stands for Neighborhood of selected building with red-dashed line.*

Table 1. Level of Importance of seven criteria (used in visual inspection of VHR images) for EMS-98 scales

Nr.	Criterion	Global Damage Grade, EMS-98				
		D1	D2	D3	D4	D5
1	Texture/Feature					
2	Color					
3	Shadow					
4	Shape/orientation					
5	Surroundings					
6	Neighborhood					
7	Usage					
Level of Importance		Low	Normal	High	Very High	

The analysis of the seven defined criteria with damage scales in EMS-98 includes an assessment of their respective importance levels for each damage grade, visualizing over 5000 buildings in VHR satellite images. The resulting findings are elaborated upon in Table 1.

Each criterion is scrutinized in its components to evaluate the level of possibility in observation (using vertical images) for each damage grade in EMS-98 classification. The relationship between these components and the defined scales for each damage class is explained in Table 2, along with further explanations as follows:

1. The possibility of cracks in walls and vertical elements of building as well as their size can be evaluated mostly by observations in texture/feature of roof, surroundings and shadow.
2. Fractures in roof and its components can be verified mostly through observations in texture/feature, color, shape/orientation and surroundings.
3. Neighborhood, surroundings, and usage can primarily assist in recognizing lower damage grades such as D1 and D2. For debris, the pattern and amount can further aid in distinguishing between these grades.
4. Partial internal failures for structural and non-structural elements can be detectable by considering observed characteristics related to texture/feature, color, shape/orientation.
5. In the case of dealing with non-visible possible pancake collapse, potential observations in color, shadow and surroundings can assist in investigation of details.
6. In some cases, the color of roof and surrounding elements can be considered to differentiate the possible damages between structural and non-structural parts.
7. Distinguishing between D1 and D2 is mostly achievable by evaluation of pattern, size and the shape of changes in texture/feature and surroundings.
8. In dense-aggregated urban areas, due to the complexities in detection of shadow and surroundings for each building, observations in texture/feature, color and shape/orientation are primarily applicable for detecting low damage grades.
9. If vertical VHR images are captured with non- adaptable high off-nadir angles, observations in texture/feature, color, surroundings and neighborhood can be mostly considered for damage detection analysis.

Table 2. Level of possibility in observed components of seven criteria (used in visual inspection of VHR images) for EMS-98 scales

No.	Criterion	Observation	Global Damage Grade				
			D1	D2	D3	D4	D5
1	Texture/Feature	Change of roof texture		O	O	O	O
		Change of roof-line width			●	●	O
		Split in roof			O	●	O
		Spot changes	O	O	O		
2	Color	Change of roof color				O	O
		Heterogeneity			O	O	O
3	Shadow	Change of shadow length			O	●	●
		Change of darkness density				O	O
		Change of roof elements shadow	O	O	●	O	O
		Change of height elements shadow			O	O	O
4	Shape/orientation	Change of footprint				O	O
		Change of roof alignment				O	O
5	Surroundings	Amount of debris	●	●	●	●	O
		Pattern	O	O	O	O	O
		Distance	O	O	O		
6	Neighborhood	Debris from adjacent buildings		O	O	O	O
		Change/Collapse of adjacent buildings			O	O	O
7	Usage	Importance of a residential building	O	O	O		
		Importance of an official building	●	●	O		

Level of possibility in observation: Empty cell: No/negligible O Low to moderate ● High

3.2. Change detection by supervised- classification

In the pre-processing phase, user-assisted supervised classification is carried out for both pre- and post-event images using the semi-automatic method facilitated by the ERDAS-IMAGINE tool. The results of the supervised classification are utilized in QGIS for pixel-based change detection analysis, and the resulting outcomes are further processed to identify changed zones in five classification.

3.3. Automatic change detection methodologies

Discriminant change detection and image difference methods were utilized as automatic image processing approaches to detect level of damages in buildings. The applied discriminant techniques for this study include Additive, Subtractive, and Combined methods, which are defined as follows:

1. Additive Discriminant Change Detection (ADCD): For a pair of corresponding pixels at the same spatial location in the pre-event (P) and post-event (Q) images, the additive change detection method calculates the change (ΔC) shown in equation (1).

$$\Delta C = |Q - P| \quad (1)$$

2. Subtractive Discriminant Change Detection (SDCD): It involves subtracting pixel values in the pre-event image from the pixel values in the post-event image displayed in equation (2).

$$\Delta C = Q - P \quad (2)$$

3. Combined Discriminant Change Detection (CDCD): It integrates information from both additive and subtractive methods to improve change detection accuracy calculated by equation (3).

$$\Delta C = |Q - P| + (Q - P) \quad (3)$$

4. Data analysis and results

Damage grade assessment through different mentioned methods are conducted on selected area in L'Aquila for about 2100 buildings coupled with evaluation of related information for structural type, number of story and vulnerability class. Figure 3 illustrates the results of the building stock survey conducted using a combination of VHR satellite images and Google Street View data. These results are then compared with the vulnerability class and damage grades assessed by Tertulliani *et al.* (2011) through ground surveys. The related legends for plots in Figure 3 are described in Table 3.

Damage classification of buildings, based on the evaluated results of automatic image processing methods, is defined in three categories that have been adjusted according to EMS-98 measures, and the related results are shown in Figure 4. The comparison procedures for the results obtained from different applied methods are performed on the following pairs of datasets:

1. VHR satellite images (criteria-based visual inspection) and Ground Survey.
2. VHR satellite images (criteria-based visual inspection) and automatic image processing methods.
3. Ground Survey and automatic image processing methods.

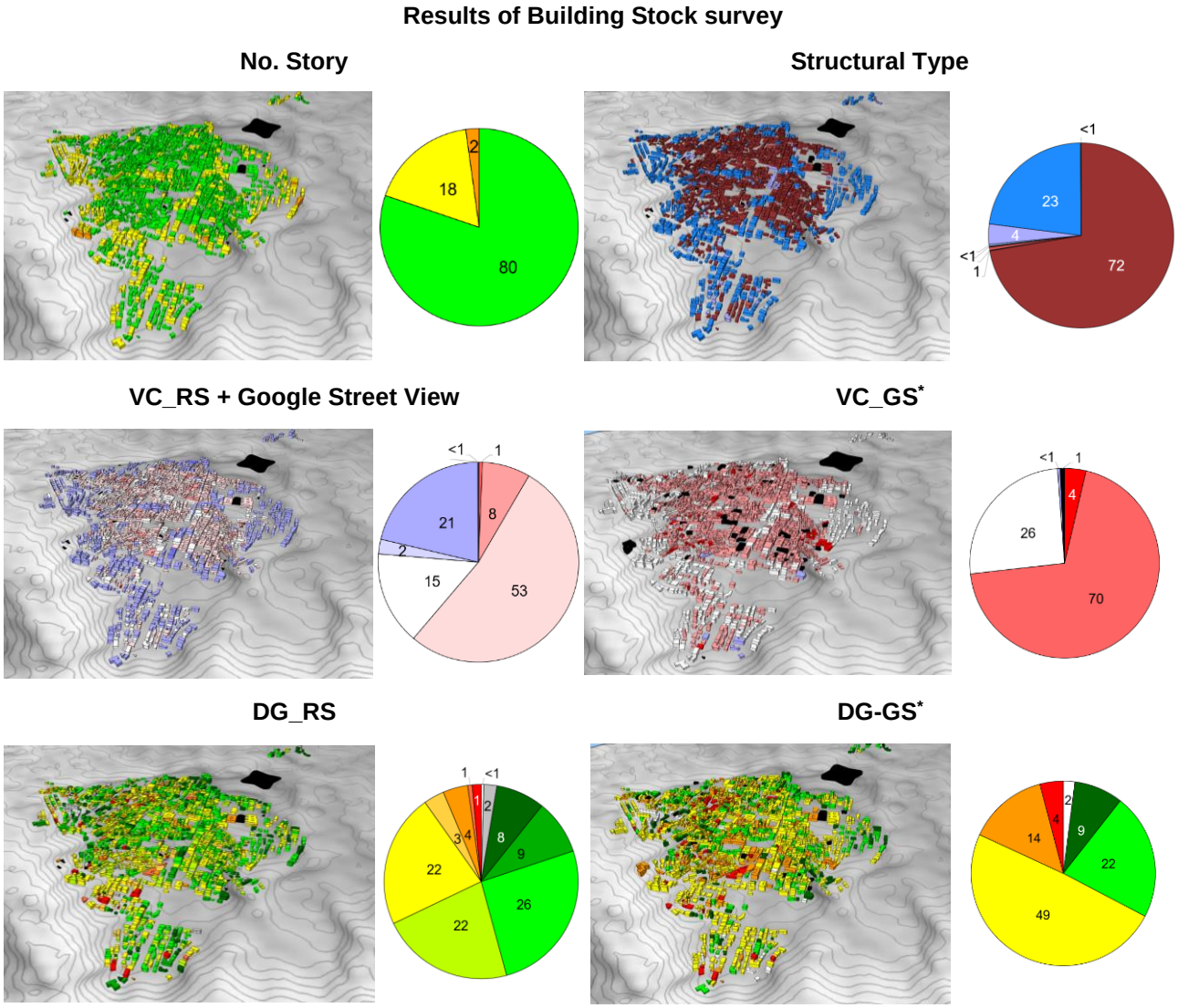

Figure 3. The results of building stock survey in L'Aquila based on criteria-based Visual inspection on VHR satellite images and ground survey

**Note: Assessed by Tertulliani et al. (2011) through Ground Surveys (GS)*

Table 3. Defined legends for building stock survey parameters in Figure 3

No. Story	1 ≤ n ≤ 3		3 < n ≤ 5		5 < n ≤ 8						
VC	A	AB	B	BC	C	CD	D	DE	E	EF	F
DG	0	0-1	1	1-2	2	2-3	3	3-4	4	4-5	5
Structural Type*	Adobe	MUR	MUR/ Sim.St.[1]	MUR/ Mass.St.[2]		MUR/C onf.	MUR/RC L_ERD		RC_L_ ERD	RC_M_ ERD	Wood

*The applied legend for structural type is based on Schwarz *et al.* (2021)
1,2 refer to Simple stone and Massive stone respectively.

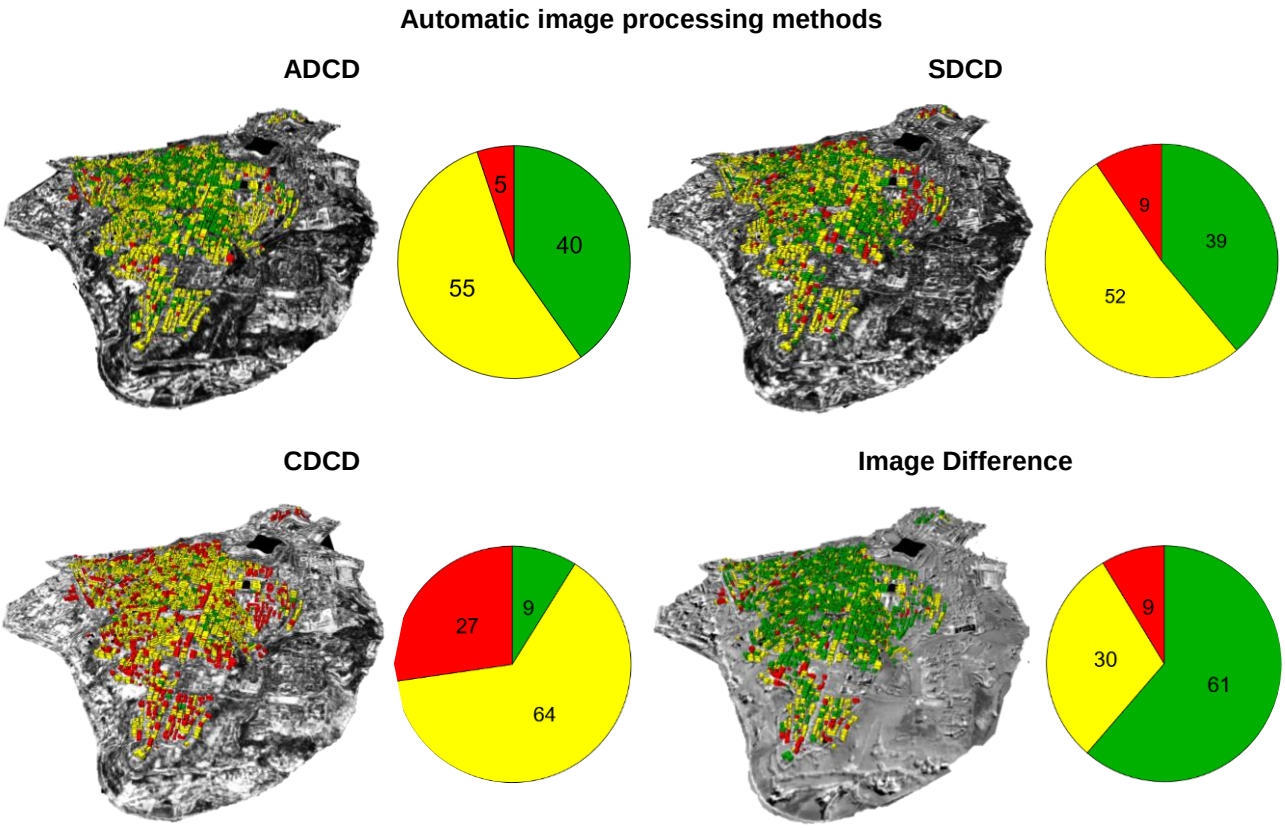

*Description: Building damage distribution are shown on processed change detection image for each method.

DG-Rapid Response			
DG-Qualitative	No-Low	Moderate-High	Very High-Total
DG-EMS-98	0 ≤ Di ≤ 2	2 < Di < 4	4 ≤ Di ≤5

Figure 4. The results of damage level assessment in L'Aquila based Automatic methods

4.1. Comparison of results between VHR satellite images and ground survey

To analyze the disparities in results between the EMS-98 criteria-based method applied to remote sensing images and the ground survey conducted by Tertulliani *et al.* (2011), two distinct approaches were employed:

1. Sampling methodologies for individual buildings.
2. Evaluation of measurements for the entire study area.

Table 4. Examples for comparison of assigned damage grade between criteria-based visual inspection method on VHR images and ground survey

Platform	Ground survey DG: D5		
	Pre-phase	**Post-phase**	**Comments**
RS	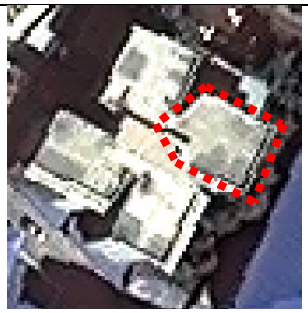		- Spot changes in roof texture & color - No differences in height considering shadow - No detection of debris **RS_DG: 1 ≤ Di < 2**
3D*			Pre- & post-phase Images show the same building with no any changes such as replacement or construction of new building.
Ground survey DG: D4			
RS			- Spot changes in roof texture & color - No changes in height - Official Building -Spot debris around **RS_DG: 1 ≤ Di < 2**
3D			Pre- & post-phase Images for white building show the same building without any changes such as replacement or construction of new building.
* 3D implies for Google Street 3D view in the case of availability.			

Table 4 provides examples of sample buildings with assigned D5 and D4 in ground surveys, along with their respective damage grades evaluated by the EMS-98 criteria-based approach on VHR satellite images, along with a comparative analysis of the differences.

Table 5 shows a comparison of damage grade assignments across the entire area. Various methods were used to evaluate the differences between measurements obtained from criteria-based visual inspections of VHR satellite images and those from ground surveys. From the several measurements applied, the following results can be concluded:

Table 5. Measurements of differences of DG and VC between criteria-based visual inspection method on VHR images (RS) and Ground Survey (GS)

Difference of DG between RS and GS

QQ-plot	Box-plot	3D-difference
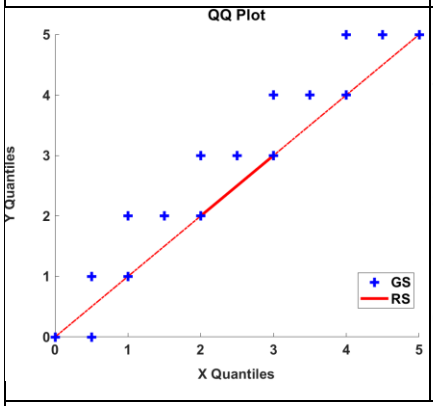	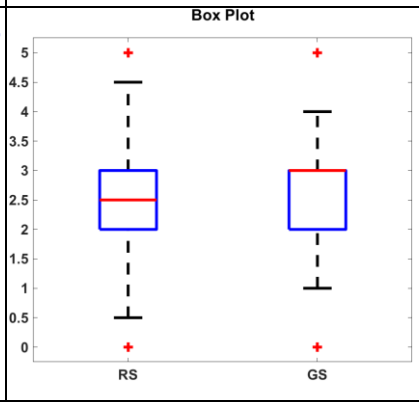	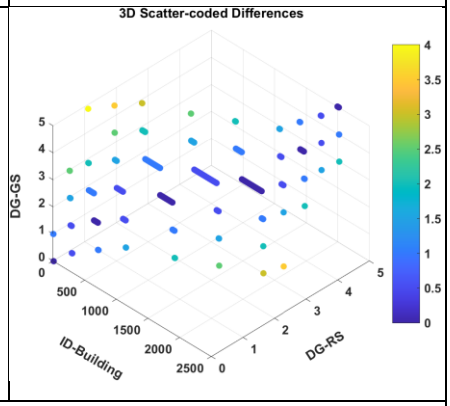

Difference of VC between RS and GS

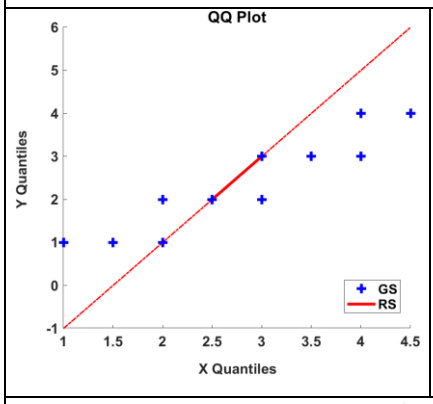	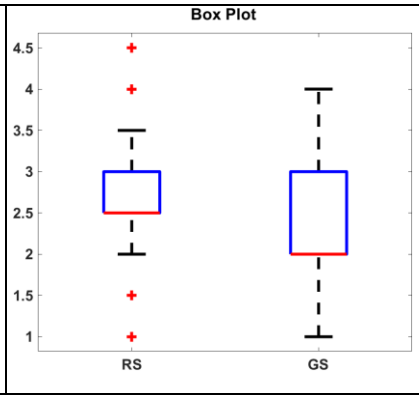	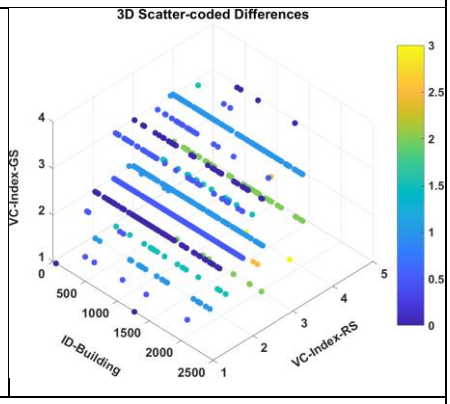

Parameters for difference measurement, Row1: DG & Row2:VC

Correlation Coefficient	RMSE	R^2	T-test: P value	Kolmogorov Smirnov: P value	Mean Distance
0.68	0.86	-0.1	0	0	0.61
0.71	0.79	0.69	0	0	0.67

VC	A	AB	B	BC	C	CD	D	DE	E	EF	F
Index	1	1.5	2	2.5	3	3.5	4	4.5	5	5.5	6

1. 3D scatter coded-plot: For damage grade measurements, while there is a broad range of “DG-GS” and “DG-RS” values across buildings, many points show low to intermediate differences between the two measurements, as evidenced by the dominant blue and green colors. There are some exceptions, particularly in the middle range of Building IDs, where the differences are more pronounced. In the measurements for vulnerability classes, there is a wide distribution of VC-Index values for “GS” and “RS” among buildings, a significant number exhibit minimal differences between these measurements, particularly in areas with a high concentration of data points. Buildings with high VC-Index values for both “GS” and “RS” are less common, and their measurement differences vary.
2. Box-plot: The distribution of damage grade data for “RS” seems to be slightly more spread out than that for “GS” with the slightly higher median than that of “GS”. The spread of vulnerability class data for “GS” is larger compared to “RS” with median value higher than that of “RS”.
3. Parameters for difference measurement: For both damage grade and vulnerability class have significant differences in their measurements based on the analyzed statistical tests, for the case of vulnerability

class, it seems to have a slightly better fit between “RS” and “GS” measurements and stronger correlation than damage grade.

4.2. Comparison of results between pairs of RS-automated and GS-automated methods

The difference analysis results between two measurement pairs — criteria-based visual inspection on remote sensing images versus automated methods, and ground survey versus automated image processing — are presented in Table 6 and Table 7 respectively which lead to the following conclusions:

1. Based on visual observations, it appears that the GS-ADCD pair might have a slightly better agreement with the ADCD method compared to RS-ADCD, especially when considering the Bland-Altman plot and the scatter plot. Additionally, For GS-ADCD, the red and blue dots seem more overlapped in scatter-plot, especially in the damage category areas of 1to 2 indicating better agreement.
2. The RS-SDCD pair seems to have more variability between the two methods compared to the GS-SDCD pair. Especially in the Bland-Altman and scatter plots, the GS-SDCD pair suggests a closer agreement between the two methods focusing range of 1to 2 in damage category.

Table 6. Measurements of differences of DG between criteria-based visual inspection method on VHR images (RS) and automatic image processing methods

Method	Scatter-plot	Bland-Altman plot	3D-Difference
ADCD	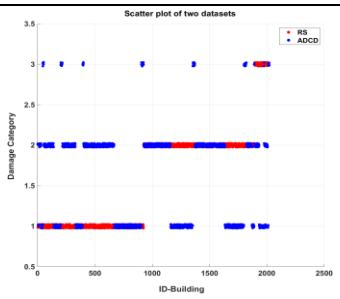	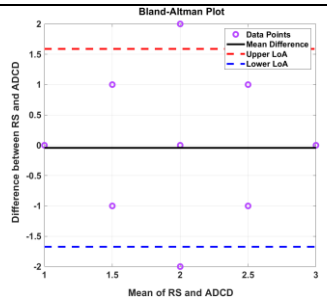	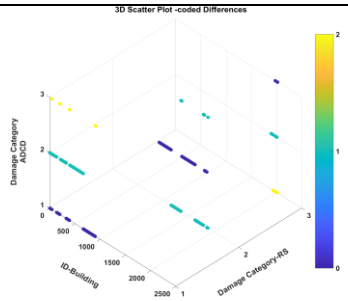
SDCD	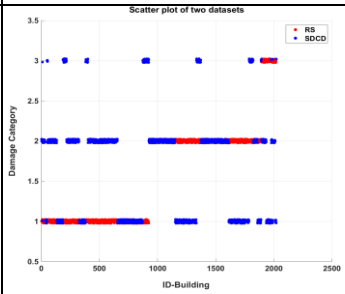	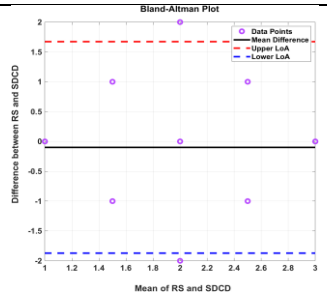	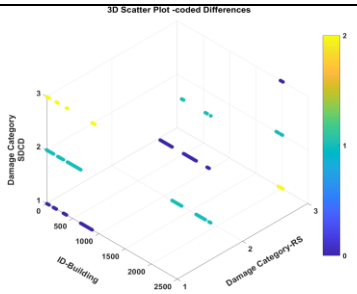
CDCD	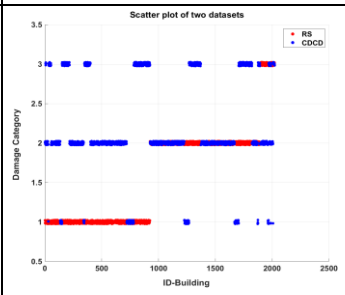	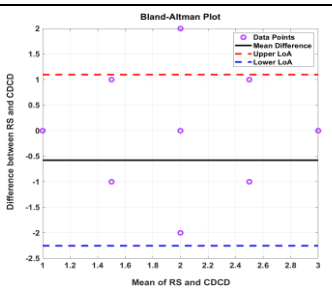	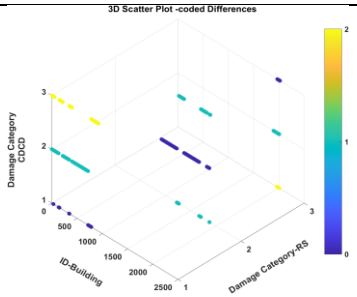
Image Difference	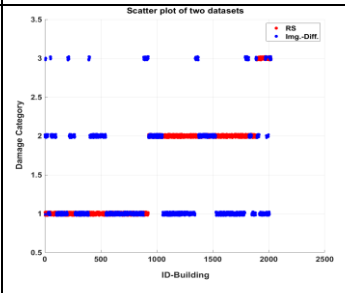	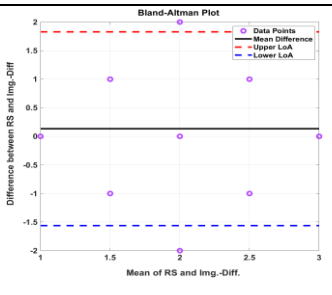	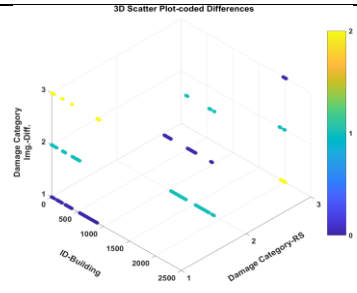

Table 7. Measurements of differences of DG between Ground Survey (GS) and automatic image processing methods

Method	Scatter-plot	Bland-Altman plot	3D-Difference
ADCD	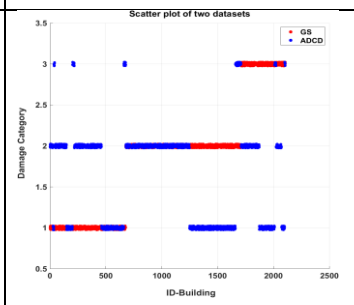	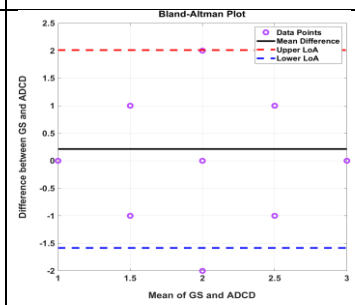	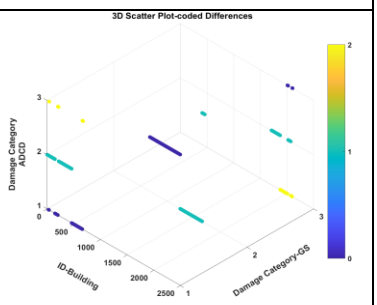
SDCD	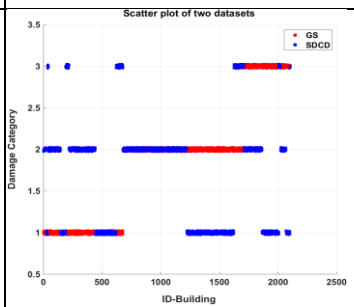	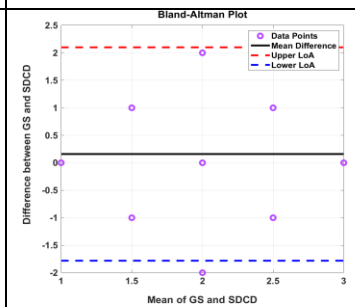	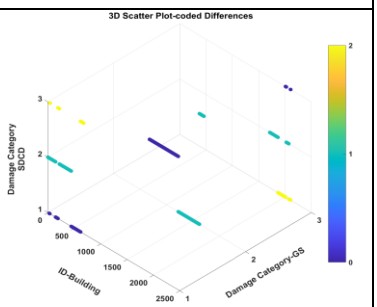
CDCD	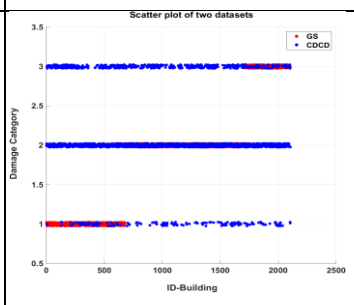	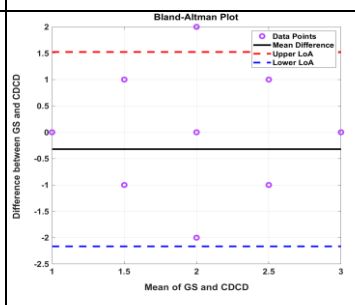	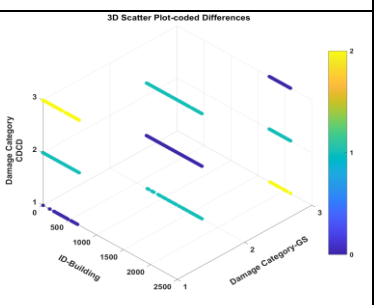
Image Difference	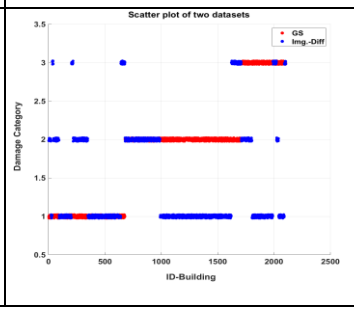	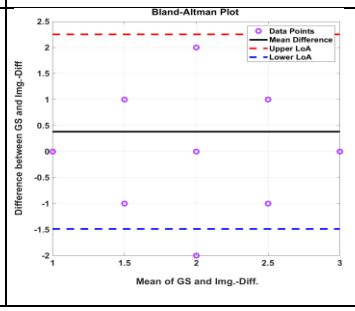	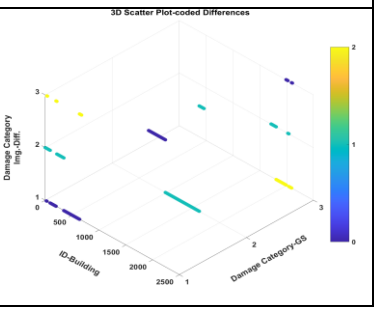

3. Both RS-CDCD and GS-CDCD pairs show a linear distribution of data points in the 3D scatter plots. Overall, while both RS and GS seem to agree with CDCD to a large extent, GS appears to have a slightly better agreement with CDCD than RS, based on the Bland-Altman plots.
4. In Image Difference method, there is good agreement with “RS” measurements mostly in damage category 1. Overall, Pair GS-Img. -Diff exhibits a high level of agreement between the "GS" and "Img. -Diff" methods, as evidenced by the close alignment of data points, minimal bias, and tight clustering within the Limits of Agreement in the Bland-Altman plot.

5. conclusion

The procedure for assessing damage to buildings in L'Aquila following the April 2009 earthquake involved two main methods: criteria-based visual inspection using two temporal VHR satellite images and automatic image processing techniques. The results obtained from both approaches were then compared with those derived from ground survey assessments. Comparing the results of damage classification obtained through ground survey with those using Google Street View (if accessible) as an ancillary checking tool revealed significant

differences in sampling methodologies and their correspondence with reality as well as with the criteria-based visual inspection method on VHR satellite images. The outcomes of automatic image processing methods exhibited a stronger agreement with ground survey damage assessments within specific damage ranges.

Overall, when comparing the results from various methodologies, it becomes evident that employing the EMS-98 criteria-based visual inspection method on VHR satellite images can increase the level of certainty in assessments. This is achieved by scrutinizing the alignment between the outcomes of the ground survey method and reality.

6. References

Contreras D., Blaschke T., Tiede D., Jilge M. (2015): Monitoring recovery after earthquakes through the integration of remote sensing, GIS, and ground observations: the case of L'Aquila (Italy), Cartography and Geographic Information Science, DOI: 10.1080/15230406.2015.1029520.

Corbane, C., Saito, K., Dell'Oro, L., Bjorgo, E., Gill, S., Emmanuel P., B., Huyck, C. K., Kemper, Th., Lemoine, G., Spence, R.J.S., Shankar, R., Senegas, O., Ghesquiere, F., Lallemant, D., Evans, G. B., Gartley, R.A., Toro, J., Ghosh, S., Svekla, W. D., Adams, B.J., Eguchi, R. T. (2011). A Comprehensive Analysis of Building Damage in the 12 January 2010 Mw7 Haiti Earthquake Using High-Resolution Satelliteand Aerial Imagery. *Photogrammetric Engineering & Remote Sensing, Number 10 / October 2011, pp.* 997-1009(13).

De Vecchi D., Dell'Acqua F. (2014). A case study on fusion of seismic damage information from space-borne and ground-based imaging of l'aquila, 2009 earthquake. *2014 IEEE Geoscience and Remote Sensing Symposium. DOI: 10.1109/IGARSS.2014.6947558.*

Grünthal, G. (ed.), Musson, R., Schwarz, J., Stucchi, M. (1998): European Macroseismic Scale 1998 (EMS-98). *Cahiers du Centre Européen de Geodynamique et de Seismologie*, Volume 15, Luxembourg 1998.

Hadidian M., N., Schwarz, J. (2022). EMS-98 based damage grade assessment using remote sensing images for cascading events. *3rd European Conference on Earthquake Engineering and Seismology*, Bucharest, Romania 4-9 September, 2022.

Kersten, J., Hadidian M. N., Kang h., Aikaterini h.,kazmi Y., manojlovski F. (2017). Object-based analysis of satellite images for building change detection after an earthquake: The case study of L'Aquila. *Bauhaus Summer School, Forecast Engineering: From Past Design to Future Decision, 20 August-1 September 2017*, Weimar, Germany.

Maiwald, H., Schwarz, J. (2020). Simulative Earthquake Damage Modelling on the Basis of EMS-98 – Realism and Predictability, *Bautechnik 97, 04, 243-254*, https://doi.org/10.1002/bate.201900064

Schwarz, J., Abrahamczyk, L., Hadidian, N., Haweyou, M., Kaufmann, Ch. (2021). Report on Knowledge-based exposure modelling framework depending on the accuracy and completeness of available data. *Version 1.0, Deliverable D4.1. TURNkey project. H2020-SC5-2018.*

Tertulliani A., Arcoraci L., Berardi M., Bernardini F., Camassi R., Castellano C., Del Mese S., Ercolani E., Graziani L., Leschiutta I., Rossi A., Vecchi M. (2011). An application of EMS98 in a medium-sized city: The case of L'Aquila (Central Italy) after the April 6, 2009 Mw 6.3 earthquake. © *Springer Science+Business Media B.V. 2010. Bull Earthquake Eng (2011) 9:67–80. DOI 10.1007/s10518-010-9188-4*.

UNOSAT (2010). Building Damage Assessment In support to Post Disaster Needs Assessment and Recovery Framework (PDNA) Haiti Earthquake 12 January 2010. Product ID: 2065, Glide: EQ20100113HTI. https://unosat.org/products/2065.

Yamazaki, f., Yano, Y., Matsuoka, M. (2005). Visual Damage Interpretation of Buildings in Bam City Using QuickBird Images Following the 2003 Bam, Iran, Earthquake. *Earthquake Spectra,* Volume 21, No. S1, pages S329–S336, December 2005; © 2005, *Earthquake Engineering Research Institute*.